

Supplemental File of “Inter-Relationship Based Selection for Decomposition Multiobjective Optimization”

Ke Li, Sam Kwong, *Fellow, IEEE*, Qingfu Zhang, *Senior Member, IEEE*, Kalyanmoy Deb, *Fellow, IEEE*

Abstract—The paper entitled “*Inter-Relationship Based Selection for Decomposition Multiobjective Optimization*” presents a simple yet effective selection operator for the decomposition-based evolutionary multiobjective optimization. By considering the mutual-preferences between subproblems and solutions (i.e., the two requirements of each agent), the selection operator is able to balance the convergence and diversity of the search process. Comprehensive experiments are conducted on several MOP test instances with complicated Pareto sets. Empirical results demonstrate the effectiveness and competitiveness of our proposed algorithm. However, due to the page limit of IEEE Transactions on Cybernetics, several issues have not been well addressed in the paper. This supplemental file is a complement of the official paper.

I. INTRODUCTION

This is the supplemental file for the paper “*Inter-Relationship Based Selection for Decomposition Multiobjective Optimization*” published in IEEE Transactions on Cybernetics. First of all, Section II presents a discussion on some properties of Tchebycheff (TCH) decomposition approach. Then, Section III gives an example of the scenario when there is no related solution for a subproblem, i.e., $\chi = \emptyset$. Afterwards, Section IV shows the empirical studies on WFG instances. At last, Section V presents the plots final solutions obtained by all seven multiobjective evolutionary algorithms (MOEAs) (i.e., MOEA/D-IR [1], MOEA/DRA [2], MOEA/D-M2M [3], MOEA/D-STM [4], MOEA/D-FRRMAB [5], HypE [6] and NSGA-II [7]) on each test instance, and Section VI shows the plots of parameter sensitivity studies.

II. DISCUSSIONS ON THE TCH APPROACH

The classic TCH approach [8] is stated as:

$$\begin{aligned} & \text{minimize } g^{tch}(\mathbf{x}|\mathbf{w}, \mathbf{z}^{**}) = \max_{1 \leq i \leq m} \{w_i \times |f_i(\mathbf{x}) - z_i^{**}| \} \\ & \text{subject to } \mathbf{x} \in \Omega \end{aligned} \quad (1)$$

K. Li is with the Department of Electrical and Computer Engineering, Michigan State University, East Lansing, MI 48824, USA (e-mail: ke-li.genius@gmail.com)

S. Kwong is with the Department of Computer Science, City University of Hong Kong, Kowloon, Hong Kong SAR. (cssamk@cityu.edu.hk)

Q. Zhang is with Department of Computer Science, City University of Hong Kong, Kowloon, Hong Kong SAR, and School of Computer Science and Electronic Engineering, University of Essex, Colchester, UK. (qingfu.zhang@cityu.edu.hk, qzhang@essex.ac.uk)

K. Deb is with the Department of Electrical and Computer Engineering, Michigan State University, East Lansing, MI 48824, USA (e-mail: kdeb@egr.msu.edu)

where $\mathbf{w} = (w_1, \dots, w_m)^T$ is a user specified weight vector, $w_i \geq 0$ for all $i \in \{1, \dots, m\}$ and $\sum_{i=1}^m w_i = 1$. $\mathbf{z}^{**} = (z_1^{**}, \dots, z_m^{**})^T$, where $z_i^{**} = z_i^* - \epsilon$ for all $i \in \{1, \dots, m\}$, $\epsilon > 0$ is a very small number, say 10^{-6} . As proved in [8], under some mild conditions, the optimal solution of (1) is a Pareto-optimal solution of the multiobjective optimization problem (MOP) in question. By altering weight vectors, TCH approach is able to find different Pareto-optimal solutions.

The reverse mapping vector of \mathbf{w} is denoted as $\bar{\mathbf{w}} = (\frac{1}{w_1} / \sum_{i=1}^m \frac{1}{w_i}, \dots, \frac{1}{w_m} / \sum_{i=1}^m \frac{1}{w_i})^T$. A line \mathbf{L} that starts from the origin and passes through $\bar{\mathbf{w}}$ is mathematically defined as:

$$\frac{t_1}{1/w_1} = \dots = \frac{t_m}{1/w_m} \quad (2)$$

where $w_i \neq 0$, $i \in \{1, \dots, m\}$. Accordingly, we have the following theorem.

Theorem 1. Let the optimal solution of (1), for an MOP with piece-wise continuous PF, with weight vector $\mathbf{w} = \{w_1, \dots, w_m\}$ is \mathbf{x} , then the intersection point of \mathbf{L} with the PF, $\mathbf{T} = (t_1, \dots, t_m)^T$, satisfies $t_i = f_i(\mathbf{x}) - z_i^{**}$, $i \in \{1, \dots, m\}$.

Proof: Assume that $\exists l \in \{1, \dots, m\}$, $t_l \neq f_l(\mathbf{x}) - z_l^{**}$. According to (1), there should exist the following two nonempty sets:

$$\begin{aligned} \Theta &= \{j | w_j \times |f_j(\mathbf{x}) - z_j^{**}| < \max_{1 \leq i \leq m} \{w_i \times |f_i(\mathbf{x}) - z_i^{**}|\}\} \\ \Phi &= \{k | w_k \times |f_k(\mathbf{x}) - z_k^{**}| = \max_{1 \leq i \leq m} \{w_i \times |f_i(\mathbf{x}) - z_i^{**}|\}\} \end{aligned} \quad (3)$$

$$\implies w_j \times |f_j(\mathbf{x}) - z_j^{**}| < w_k \times |f_k(\mathbf{x}) - z_k^{**}| \quad (4)$$

where $j \in \Theta$ and $k \in \Phi$.

Since the MOP, in question, is piece-wise continuous, suppose that there is another solution \mathbf{x}' , whose corresponding objective vector is $\mathbf{F}(\mathbf{x}') = (f_1(\mathbf{x}'), \dots, f_m(\mathbf{x}')^T$ and $\mathbf{F}(\mathbf{x}')$ is in the ϵ -neighborhood of $\mathbf{F}(\mathbf{x})$. In addition, we assume that $f_j(\mathbf{x}') > f_j(\mathbf{x})$, $j \in \Theta$, and $f_k(\mathbf{x}') < f_k(\mathbf{x})$, $k \in \Phi$. According to equation (3), we have $w_j \times |f_j(\mathbf{x}) - z_j^{**}| < w_j \times |f_j(\mathbf{x}') - z_j^{**}| < w_k \times |f_k(\mathbf{x}') - z_k^{**}| < w_k \times |f_k(\mathbf{x}) - z_k^{**}|$.

$$\implies g^{tch}(\mathbf{x}'|\mathbf{w}, \mathbf{z}^{**}) = \max_{1 \leq i \leq m} \{w_i \times |f_i(\mathbf{x}') - z_i^{**}|\} \quad (5)$$

$$= w_k \times |f_k(\mathbf{x}') - z_k^{**}| \quad (6)$$

$$< w_k \times |f_k(\mathbf{x}) - z_k^{**}| \quad (7)$$

$$= \max_{1 \leq i \leq m} \{w_i \times |f_i(\mathbf{x}) - z_i^{**}|\} \quad (8)$$

$$= g^{tch}(\mathbf{x}|\mathbf{w}, \mathbf{z}^{**})$$

where $k \in \Phi$. This obviously violates the condition that \mathbf{x} is the optimal solution of the TCH function with weight vector \mathbf{w} . ■

Theorem 1 implies that the search direction of the TCH approach is the reverse mapping vector of the corresponding weight vector as shown in Figure 1. In order to make the search direction of TCH approach become the reverse mapping vector, we make a simple modification on (1) as follows:

$$\begin{aligned} \text{minimize } & g^{tch2}(\mathbf{x}|\mathbf{w}, \mathbf{z}^{**}) = \max_{1 \leq i \leq m} \{|f_i(\mathbf{x}) - z_i^{**}|/w_i\} \\ \text{subject to } & \mathbf{x} \in \Omega \end{aligned} \quad (9)$$

where w_i is set to be a very small number, say 10^{-6} , in case $w_i = 0$.

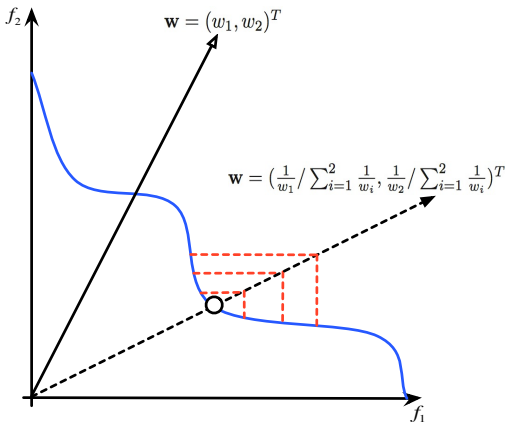


Fig. 1: Illustration of the TCH approach

III. EXAMPLE OF EMPTY χ

Consider the example shown in Figure 2, let $K_d = \vartheta = 3$, according to Algorithm 2 of our paper [1], we may have χ^5 be an empty set. For better understanding, the pseudo-code of evaluating the mutual-preferences between subproblems and solutions is given in Algorithm 1.

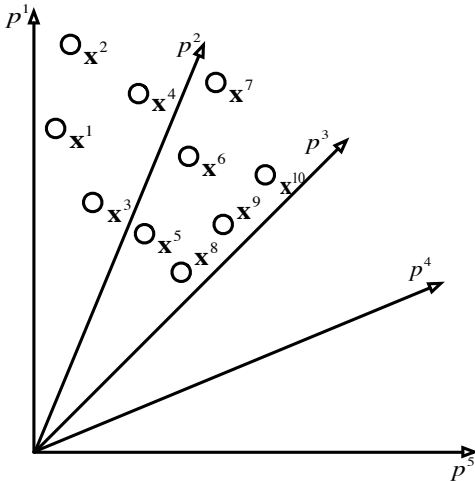


Fig. 2: Illustration of empty χ , where $\chi^5 = \emptyset$.

Algorithm 1: COMPTPREF($S, P, \mathbf{z}^*, \mathbf{z}^{nad}$)

Input: solution set S , subproblem set P , the ideal and nadir objective vectors \mathbf{z}^* , \mathbf{z}^{nad}
Output: preference matrices Δ_X and Δ_P , distance ordering matrix Ψ_{d^\perp}

```

1 for  $i \leftarrow 1$  to  $M$  do
2   |    $\bar{\mathbf{F}}(\mathbf{x}^i) \leftarrow \frac{\mathbf{F}(\mathbf{x}^i) - \mathbf{z}^*}{\mathbf{z}^{nad} - \mathbf{z}^*}$ ;
3 end
4 for  $i \leftarrow 1$  to  $M$  do
5   |   for  $j \leftarrow 1$  to  $N$  do
6     |     |    $\Delta_P(p^j, \mathbf{x}^i) \leftarrow g(\mathbf{x}^i | \mathbf{w}^j, \mathbf{z}^*)$ ;
7     |     |    $d^\perp(\mathbf{x}^i, p^j) \leftarrow \bar{\mathbf{F}}(\mathbf{x}^i) - \frac{\mathbf{w}^{jT}\bar{\mathbf{F}}(\mathbf{x}^i)}{\mathbf{w}^{jT}\mathbf{w}^j}\mathbf{w}^j$ ;
8   |   end
9 end
10 Sort each row of  $d^\perp$  in ascending order and keep the sorted indices in  $\Psi_{d^\perp}$ ;
11 for  $i \leftarrow 1$  to  $N$  do
12   |    $nc[i] \leftarrow 0$ ;
13 end
14 Normalize  $d^\perp$  and  $nc$  to range  $[0, 1]$  respectively;
15 for  $i \leftarrow 1$  to  $M$  do
16   |    $nc[\Psi_{d^\perp}(i, 1)] \leftarrow nc[\Psi_{d^\perp}(i, 1)] + 1$ ;
17 end
18 for  $i \leftarrow 1$  to  $M$  do
19   |   for  $j \leftarrow 1$  to  $N$  do
20     |     |    $\Delta_X(\mathbf{x}^i, p^j) \leftarrow d^\perp(\mathbf{x}^i, p^j) + nc(j)$ ;
21   |   end
22 end
23 return  $\Delta_X, \Delta_P, \Psi_{d^\perp}$ 

```

IV. PERFORMANCE COMPARISONS ON WFG INSTANCES

Table I and Table II present the IGD and HV metric values obtained by seven MOEAs on all WFG instances. From these empirical results, it is clear that the performance of MOEA/D-IR is better than the other algorithms. It obtains the better metric values in 89 out of 108 comparisons. According to the Wilcoxon's rank sum tests, 80 of these better results are with statistical significance. Similar to the observations on UF and MOP instances, the differences of metric values obtained by MOEA/D-IR and MOEA/D-STM are not significant on many WFG instances, especially for WFG6, WFG7 and WFG9. In the supplemental file, Figure 10 presents the non-dominated fronts obtained by these seven MOEAs. From those nine subfigures, we notice that the differences between these seven algorithms are not significant in most cases. WFG1 is a difficult test instance with a strong bias away from the PF. From Figure 10, we find that only the non-dominated fronts obtained by MOEA/D-IR and MOEA/D-FRRMAB well converge to the PF and have a satisfied distribution along the PF. Although the non-dominated front obtained by MOEA/D-STM approximate the entire PF, the convergence is not as good as those of MOEA/D-IR and MOEA/D-FRRMAB. In contrast, the other algorithms can hardly find a well converged non-dominated fronts. The PF of WFG2 consists of five disconnected segments. Almost all algorithms have no

Algorithm 2: INTERRELATION(Δ_X, Ψ_{d^\perp})

Input: preference matrix Δ_X , distance ordering matrix Ψ_{d^\perp}

Output: list of related solutions of subproblems χ

- 1 Sort each row of Δ_X in ascending order and keep the sorted indices in Ψ_X ;
- 2 **for** $i \leftarrow 1$ **to** N **do**
- 3 **for** $j \leftarrow 1$ **to** M **do**
- 4 **for** $k \leftarrow 1$ **to** K_d **do**
- 5 **if** $\Psi_X(j, k) = i$ **then**
- 6 | $\chi[i].add(j)$;
- 7 **end**
- 8 **end**
- 9 **end**
- 10 **end**
- 11 **for** $i \leftarrow 1$ **to** N **do**
- 12 **if** $\chi[i].size > \vartheta$ **then**
- 13 | Keep the ϑ ones in $\chi[i]$ that have the highest ranks in Ψ_{d^\perp} ;
- 14 **end**
- 15 **end**
- 16 **return** χ

difficulty on this test instance. However, some solutions found by MOEA/D-IR do not converge to the PF, while HypE cannot find solutions on the rightmost segment. WFG4 to WFG9 have the same PF shape. On WFG4 to WFG7 and WFG9, the non-dominated fronts found by these seven algorithms are not visually different. However, we notice that HypE usually find the extreme points of the PF, but lose some intermediate parts along the PF. WFG8 is a difficult problem, all algorithms cannot find a well converged non-dominated front. However, solutions found by MOEA/D-IR have a better convergence and diversity.

Moreover, Table III presents the experimental results of MOEA/D-IR and its two variants suggested in Section VII-C of our paper on WFG instances. Similar to the observations on UF and MOP instances, our proposed selection operator shows the best performance in most comparisons.

V. PLOTS OF SOLUTION SETS

Figure 3 to Figure 10 plot the final solutions obtained by MOEA/D-IR and the other six MOEAs on each of UF, MOP and WFG instances.

VI. PLOTS OF PARAMETER SENSITIVITY STUDIES

Figure 11 and Figure 12 show the plot of median IGD values found by different parameter combinations of K_d and ϑ on each of UF, MOP and WFG instances.

REFERENCES

- [1] K. Li, S. Kwong, Q. Zhang, and K. Deb, "Inter-relationship based selection for decomposition multiobjective optimization," *IEEE Transactions on Cybernetics*, 2014, accepted for publication.
- [2] Q. Zhang, W. Liu, and H. Li, "The performance of a new version of moea/d on cec09 unconstrained mop test instances," in *CEC'09: Proc. of the 2009 IEEE Congress on Evolutionary Computation*, 2009, pp. 203–208.
- [3] H.-L. Liu, F. Gu, and Q. Zhang, "Decomposition of a multiobjective optimization problem into a number of simple multiobjective subproblems," *IEEE Transactions on Evolutionary Computation*, vol. 18, no. 3, pp. 450–455, Jun. 2014.
- [4] K. Li, Q. Zhang, S. Kwong, M. Li, and R. Wang, "Stable matching based selection in evolutionary multiobjective optimization," *IEEE Transactions on Evolutionary Computation*, 2013, accepted for publication.
- [5] K. Li, Á. Fialho, S. Kwong, and Q. Zhang, "Adaptive operator selection with bandits for multiobjective evolutionary algorithm based decomposition," *IEEE Transactions on Evolutionary Computation*, no. 1, pp. 114–130, Feb. 2014.
- [6] J. Bader and E. Zitzler, "HypE: An algorithm for fast hypervolume-based many-objective optimization," *Evolutionary Computation*, vol. 19, no. 1, pp. 45–76, 2011.
- [7] K. Deb, A. Pratap, S. Agarwal, and T. Meyarivan, "A fast and elitist multiobjective genetic algorithm: NSGA-II," *IEEE Transactions on Evolutionary Computation*, vol. 6, no. 2, pp. 182–197, Apr. 2002.
- [8] K. Miettinen, *Nonlinear Multiobjective Optimization*. Kluwer Academic Publisher, 1999, vol. 12.

TABLE I: Performance comparisons of IGD values on WFG test instances

Test Instance	MOEA/D-IR	MOEA/D-DRA	MOEA/D-FRRMAB	MOEA/D-M2M	MOEA/D-STM	HypE	NSGA-II
WFG1	1.166E-1(4.05E-2)	2.117E-1(9.10E-2) [†]	1.250E-1(5.45E-2) [†]	1.610E-1(5.63E-2) [†]	1.277E-1(4.68E-2) [†]	3.389E-1(2.49E-1) [†]	4.146E-1(1.02E-1) [†]
WFG2	3.681E-2(4.07E-4)	3.560E-2(1.25E-3) [‡]	3.591E-2(2.75E-4) [‡]	3.891E-2(3.05E-4) [†]	3.562E-2(1.25E-2) [‡]	7.296E-2(1.02E-2) [†]	1.179E-2(6.01E-4)[‡]
WFG3	1.097E-2(2.36E-5)	1.297E-2(2.08E-5) [†]	1.298E-2(1.79E-5) [†]	1.498E-2(1.79E-5) [†]	1.296E-2(2.00E-5) [†]	1.286E-2(2.01E-4) [†]	1.575E-2(7.14E-4) [†]
WFG4	1.382E-2(2.26E-3)	1.652E-2(8.32E-4) [†]	1.771E-2(1.80E-3) [†]	2.803E-2(3.12E-3) [†]	1.600E-2(4.34E-4) [†]	1.836E-2(9.68E-4) [†]	1.442E-2(7.92E-4) [†]
WFG5	6.854E-2(5.95E-4)	6.648E-2(3.14E-3)[‡]	6.717E-2(1.52E-5) [‡]	6.801E-2(3.17E-4)	6.718E-2(4.15E-5) [‡]	7.156E-2(6.44E-4) [†]	6.748E-2(4.39E-4) [‡]
WFG6	1.544E-2(2.08E-5)	1.547E-2(2.88E-5)	1.546E-2(2.91E-5)	1.596E-2(5.77E-4) [†]	1.545E-2(2.84E-5)	4.229E-2(2.34E-2) [†]	1.625E-2(7.33E-4) [†]
WFG7	1.563E-2(1.95E-5)	1.562E-2(1.65E-5)	1.662E-2(8.73E-6)	1.687E-2(7.22E-4) [†]	1.563E-2(1.09E-5)	2.100E-2(8.98E-4) [†]	1.709E-2(8.79E-4) [†]
WFG8	1.447E-1(5.57E-2)	1.562E-1(1.65E-2) [†]	1.587E-1(4.83E-2) [†]	1.901E-1(3.58E-2) [†]	1.547E-1(5.94E-2) [†]	1.872E-1(3.73E-2) [†]	1.801E-1(1.55E-2) [†]
WFG9	1.515E-2(8.17E-4)	1.619E-2(8.82E-4) [†]	1.763E-1(5.88E-2) [†]	1.963E-2(6.17E-4) [†]	1.512E-2(3.97E-4)	1.996E-2(7.53E-4) [†]	1.942E-2(1.37E-3) [†]

Wilcoxon's rank sum test at a 0.05 significance level is performed between MOEA/D-IR and each of the other MOEAs. [†] and [‡] denotes that the performance of the corresponding algorithm is significantly worse than or better than that of MOEA/D-IR, respectively. The best mean is highlighted in boldface with gray background.

TABLE II: Performance comparisons of HV values on WFG test instances

Test Instance	MOEA/D-IR	MOEA/D-DRA	MOEA/D-FRRMAB	MOEA/D-M2M	MOEA/D-STM	HypE	NSGA-II
WFG1	11.6325(6.14E-1)	10.3021(5.60E-1) [†]	11.0056(6.01E-1) [†]	10.8256(6.28E-1) [†]	10.7506(2.45E-1) [†]	9.0128(5.48E-1) [†]	9.7436(1.77E+0) [†]
WFG2	11.4030(1.88E-1)	11.4445(9.10E-4) [‡]	11.4405(5.31E-4) [‡]	11.3455(6.11E-4) [†]	11.4440(1.31E-3) [‡]	10.9607(4.13E-1) [†]	11.4522(9.57E-4)[‡]
WFG3	10.9596(6.55E-4)	10.9494(7.89E-4) [†]	10.9493(4.27E-4) [†]	10.9461(4.82E-4) [†]	10.9495(9.85E-4) [†]	10.9245(2.45E-3) [†]	10.9494(3.14E-3) [†]
WFG4	8.6540(2.82E-2)	8.6345(1.80E-2) [†]	8.6262(1.63E-2) [†]	8.5493(5.00E-4) [†]	8.6462(1.24E-2) [†]	8.6229(1.26E-2) [†]	8.6266(1.65E-3) [†]
WFG5	8.1348(2.38E-2)	8.1336(1.73E-2) [†]	8.1325(6.77E-4) [†]	8.1359(3.14E-2) [‡]	8.1379(1.74E-2) [‡]	8.1358(2.49E-2) [‡]	8.1925(2.81E-2)[‡]
WFG6	8.6729(1.06E-3)	8.6726(6.88E-4)	8.6723(2.57E-4)	8.6697(1.61E-4) [†]	8.6727(7.42E-4)	8.4882(1.68E-1) [†]	8.6627(1.70E-3) [†]
WFG7	8.6742(4.31E-4)	8.6740(4.24E-4)	8.6688(3.87E-4)	8.6683(2.71E-4) [†]	8.6741(2.74E-4)	8.6590(3.08E-3) [†]	8.6674(1.24E-3) [†]
WFG8	7.2441(5.72E-1)	7.2040(4.24E-1) [†]	7.1117(5.21E-1) [†]	6.9081(4.85E-1) [†]	7.2432(5.45E-1) [†]	7.0111(5.28E-1) [†]	6.9139(2.42E-1) [†]
WFG9	8.4353(3.11E-2)	8.4299(9.91E-3) [†]	7.1058(4.19E-1) [†]	8.4100(1.65E-2) [†]	8.4530(7.48E-3)[‡]	8.4101(2.39E-2) [†]	8.4161(1.74E-2) [†]

Wilcoxon's rank sum test at a 0.05 significance level is performed between MOEA/D-IR and each of the other MOEAs. [†] and [‡] denotes that the performance of the corresponding algorithm is significantly worse than or better than that of MOEA/D-IR, respectively. The best mean is highlighted in boldface with gray background.

TABLE III: Performance comparisons of MOEA/D-IR and two variants

Test Instance	IGD			HV		
	MOEA/D-IR	Variant-I	Variant-II	MOEA/D-IR	Variant-I	Variant-II
WFG1	1.166E-1(4.05E-2)	1.317E+0(5.13E-2) [†]	1.177E-1(4.05E-2) [†]	11.6325(6.14E-1)	4.1055(2.71E-1) [†]	11.3993(7.52E-1) [†]
WFG2	3.481E-2(4.07E-4)	5.885E-1(8.22E-2) [†]	3.477E-2(2.29E-3)	11.4030(1.88E-1)	7.5054(4.43E-1) [†]	11.2795(3.40E-1) [†]
WFG3	1.097E-2(2.36E-5)	5.091E-1(4.71E-2) [†]	1.296E-2(2.15E-5) [†]	10.9596(6.55E-4)	7.2916(2.82E-1) [†]	10.9497(6.02E-4) [†]
WFG4	1.382E-2(2.26E-3)	2.921E-1(3.15E-2) [†]	1.589E-2(3.01E-4) [†]	8.6540(2.82E-2)	6.4075(2.42E-1) [†]	8.6492(9.73E-3) [†]
WFG5	6.854E-2(5.95E-4)	2.828E-1(3.86E-2) [†]	6.719E-2(4.29E-5)[‡]	8.1348(2.38E-2)	6.3418(2.77E-1) [†]	8.1453(2.46E-2)[‡]
WFG6	1.544E-2(2.08E-5)	5.317E-1(5.91E-2) [†]	1.646E-2(2.60E-5) [†]	8.6729(1.06E-3)	4.9292(3.93E-1) [†]	8.6706(1.01E-3) [†]
WFG7	1.562E-2(1.95E-5)	4.796E-1(1.08E-1) [†]	1.762E-2(1.16E-5) [†]	8.6742(4.31E-4)	5.3557(5.14E-1) [†]	8.6700(4.53E-4) [†]
WFG8	1.447E-1(5.57E-2)	6.455E-1(5.11E-2) [†]	1.770E-1(4.35E-2) [†]	7.2441(5.72E-1)	4.0060(2.31E-1) [†]	7.1215(4.53E-1) [†]
WFG9	1.515E-2(8.17E-4)	4.906E-1(8.24E-2) [†]	1.611E-2(5.33E-4) [†]	8.4353(3.11E-2)	5.3224(4.76E-1) [†]	8.4527(1.02E-2)[‡]

Wilcoxon's rank sum test at a 0.05 significance level is performed between MOEA/D-IR and each of the two variants. [†] and [‡] denotes that the performance of the corresponding algorithm is significantly worse than or better than that of MOEA/D-IR, respectively. The best mean is highlighted in boldface with gray background.

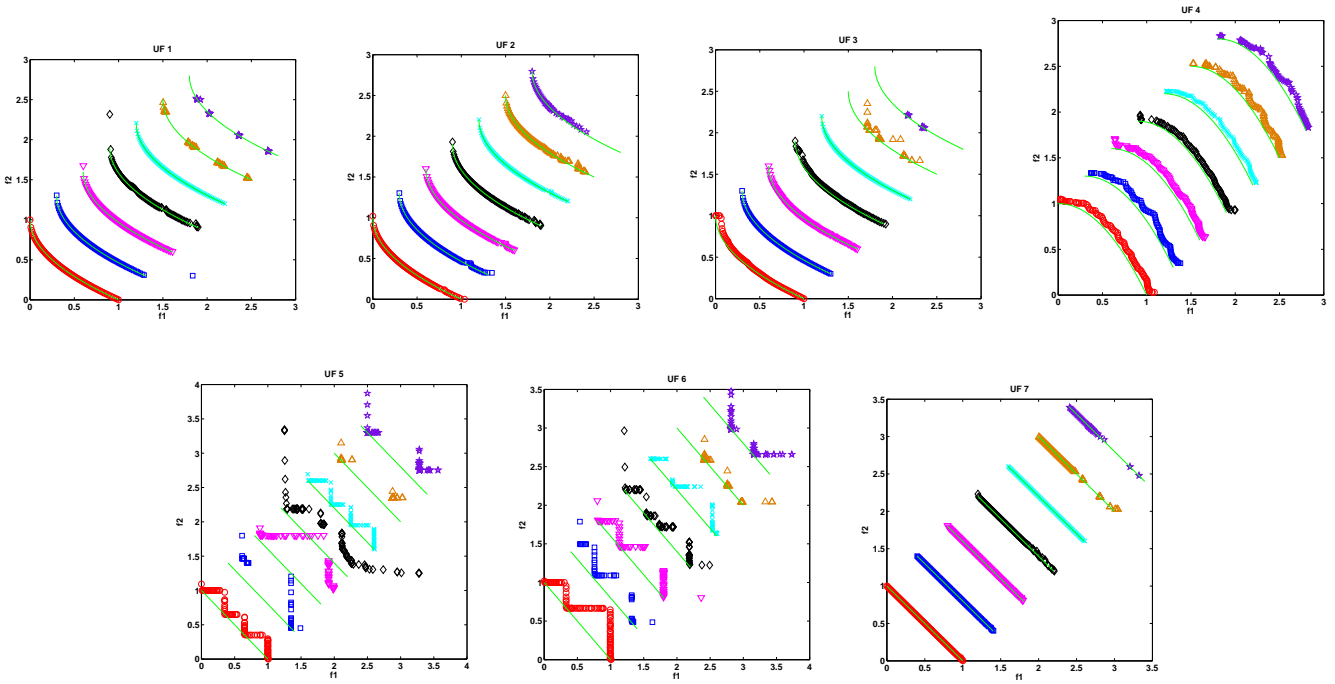


Fig. 3: Plots of the non-dominated front with the median IGD value found by each of MOEA/D-IR and the other MOEAs on UF1 to UF7.

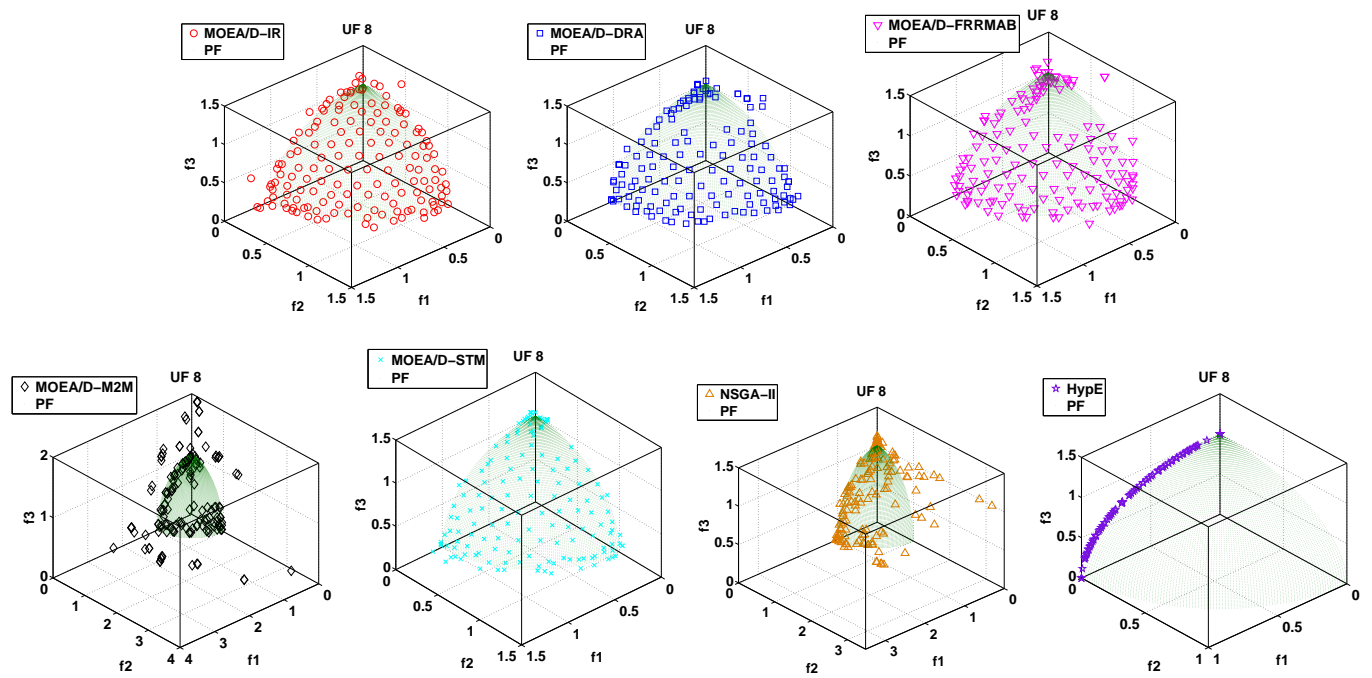


Fig. 4: Plots of the non-dominated front with the median IGD value found by each of MOEA/D-IR and the other MOEAs on UF8.

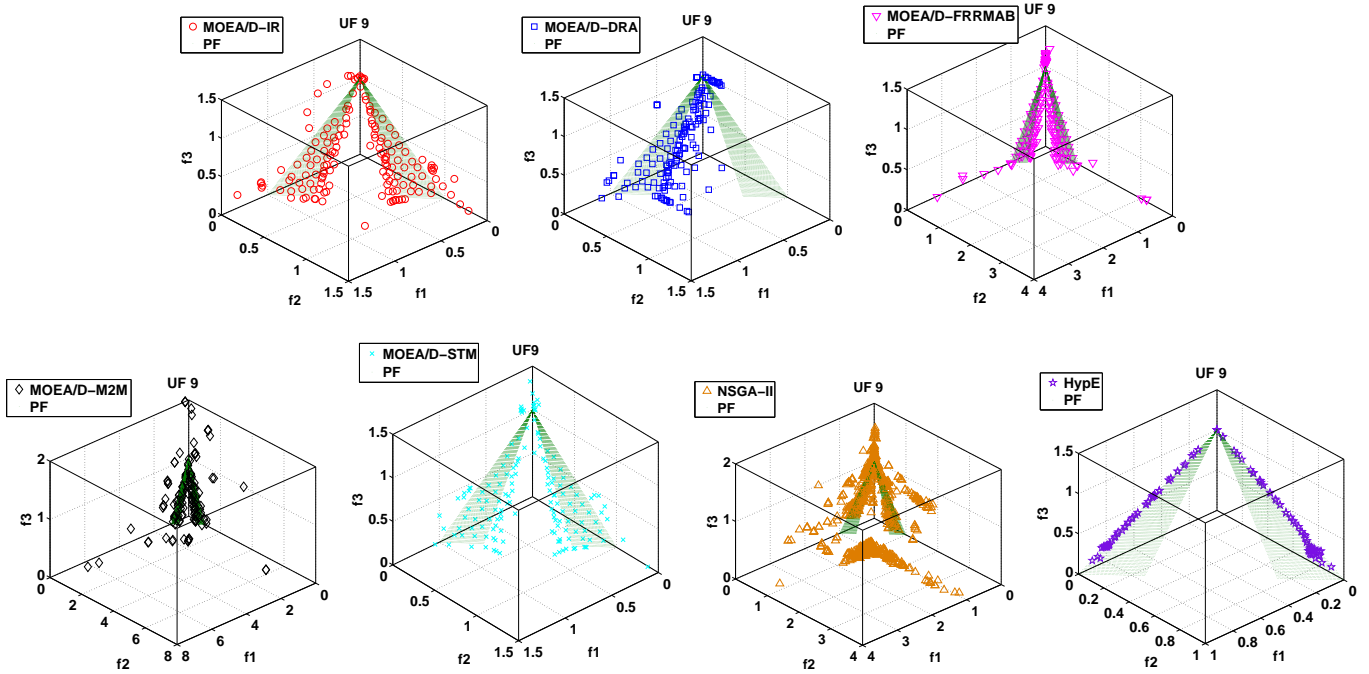


Fig. 5: Plots of the non-dominated front with the median IGD value found by each of MOEA/D-IR and the other MOEAs on UF9.

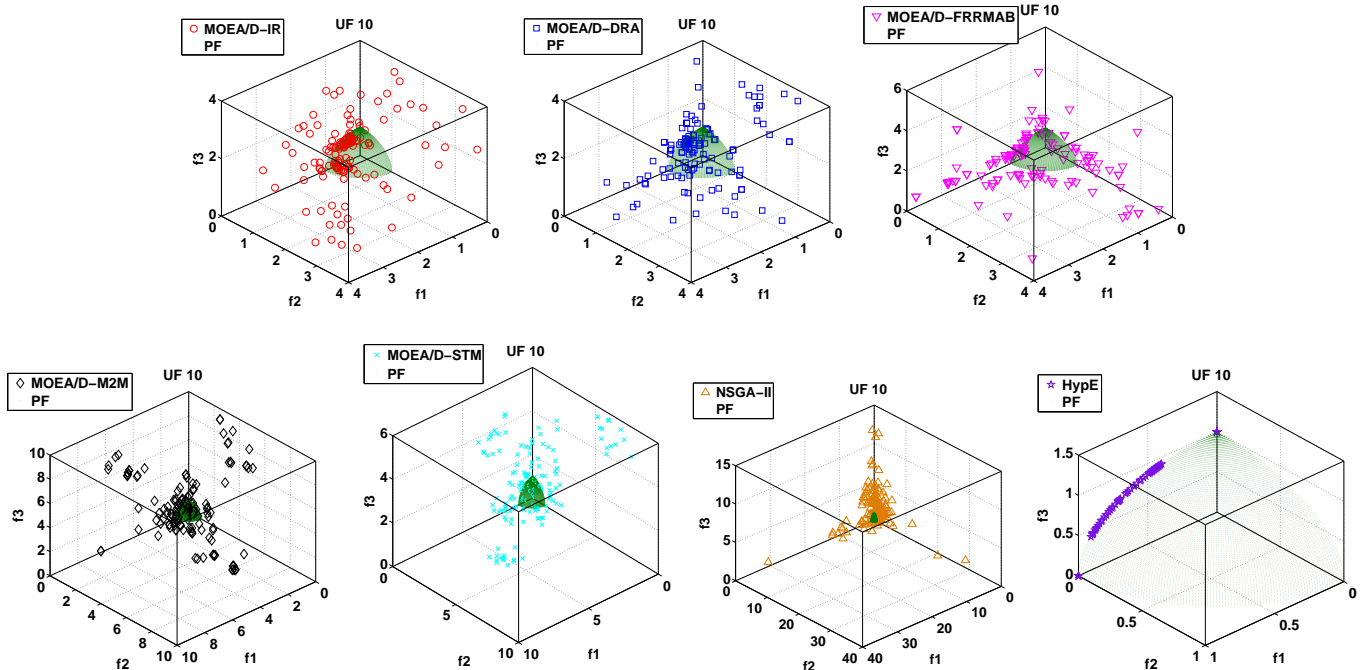


Fig. 6: Plots of the non-dominated front with the median IGD value found by each of MOEA/D-IR and the other MOEAs on UF10.

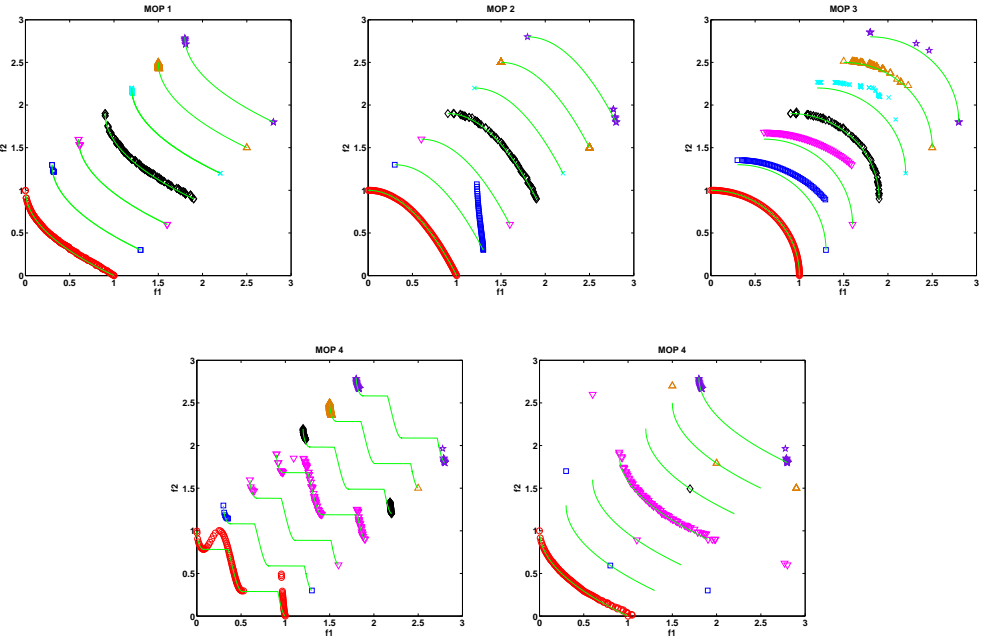


Fig. 7: Plots of the non-dominated front with the median IGD value found by each of MOEA/D-IR and the other MOEAs on MOP1 to MOP5.

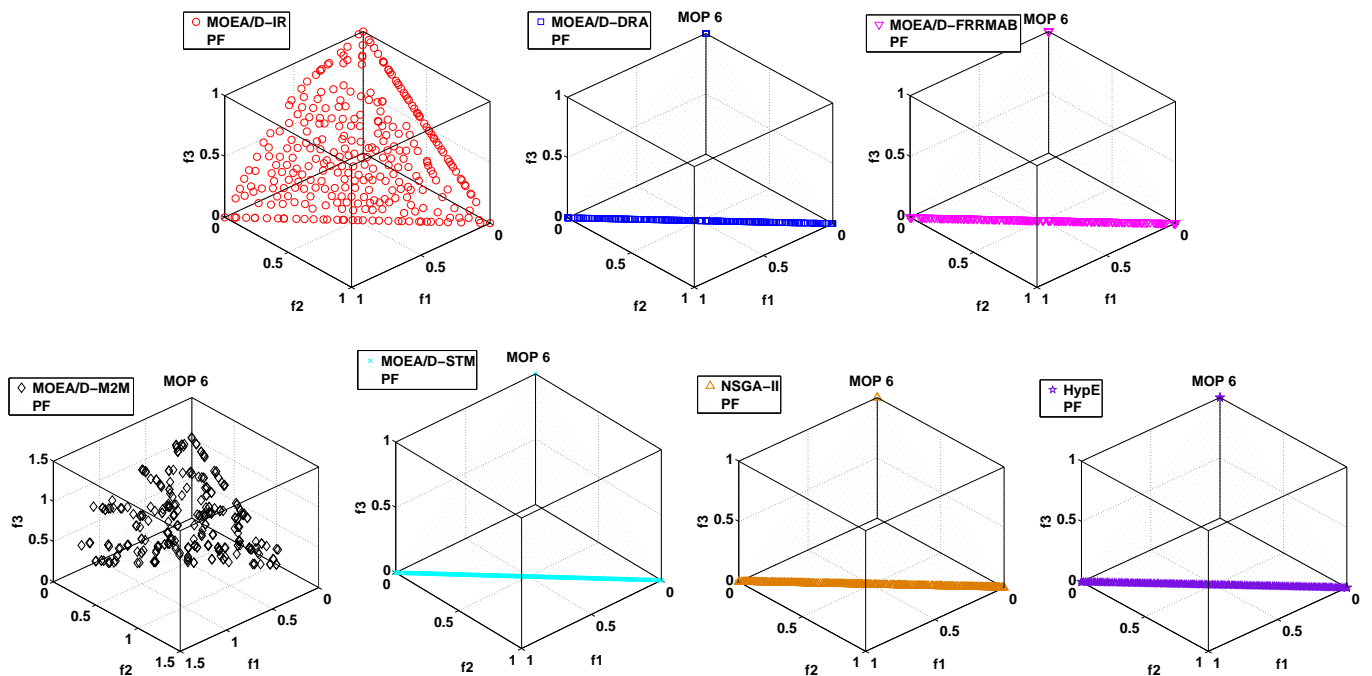


Fig. 8: Plots of the non-dominated front with the median IGD value found by each of MOEA/D-IR and the other MOEAs on MOP6.

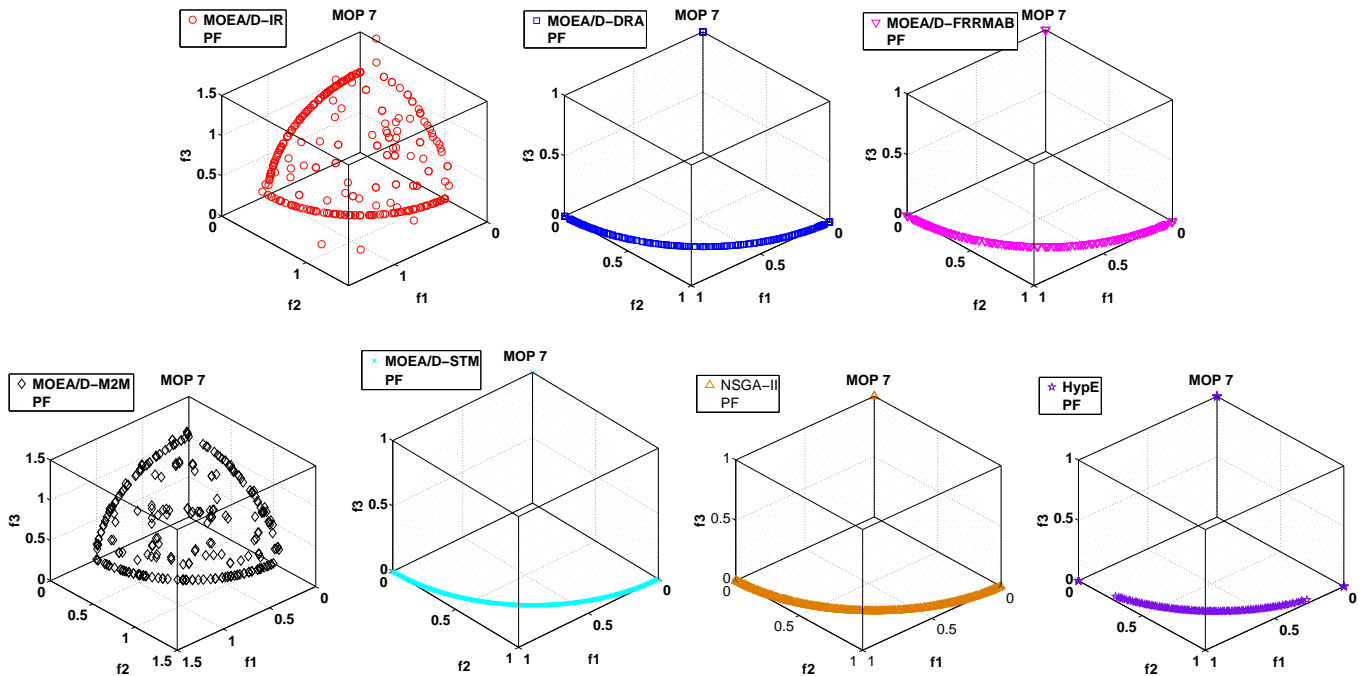


Fig. 9: Plots of the non-dominated front with the median IGD value found by each of MOEA/D-IR and the other MOEAs on MOP7.

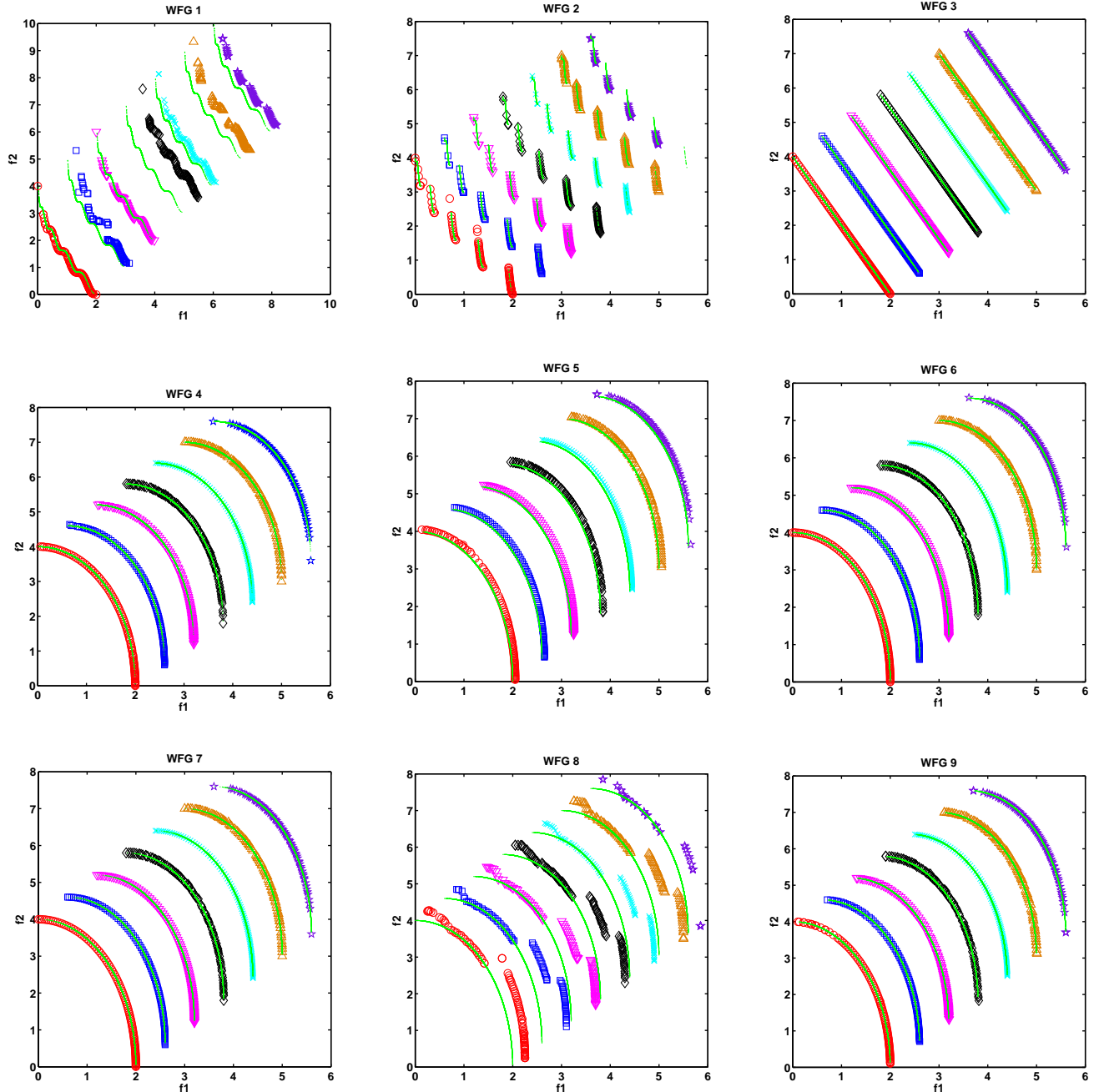


Fig. 10: Plots of the non-dominated front with the median IGD value found by each of MOEA/D-IR and the other MOEAs on WFG1 to WFG9.

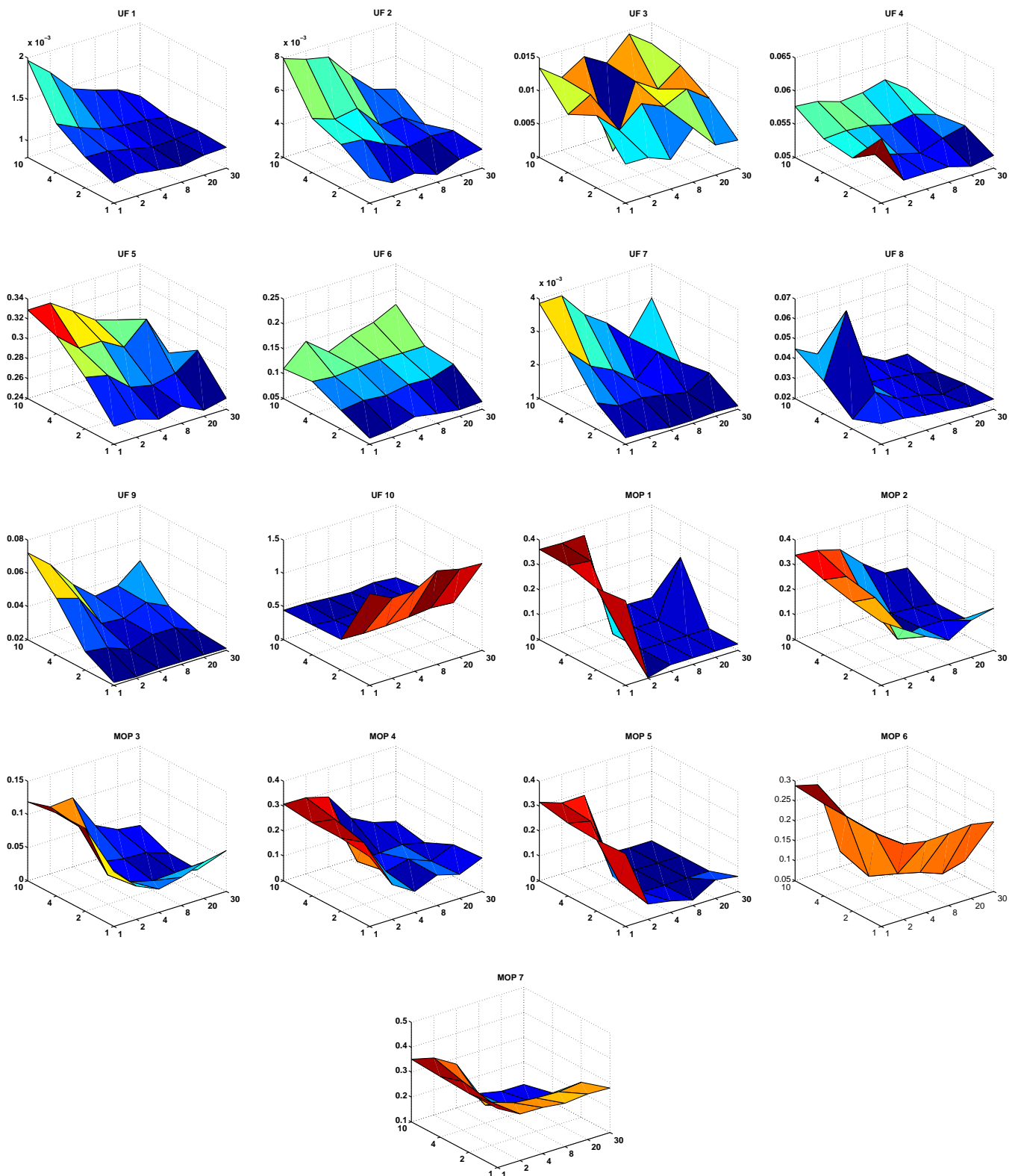


Fig. 11: Parameter sensitivity studies of K_d and ϑ .

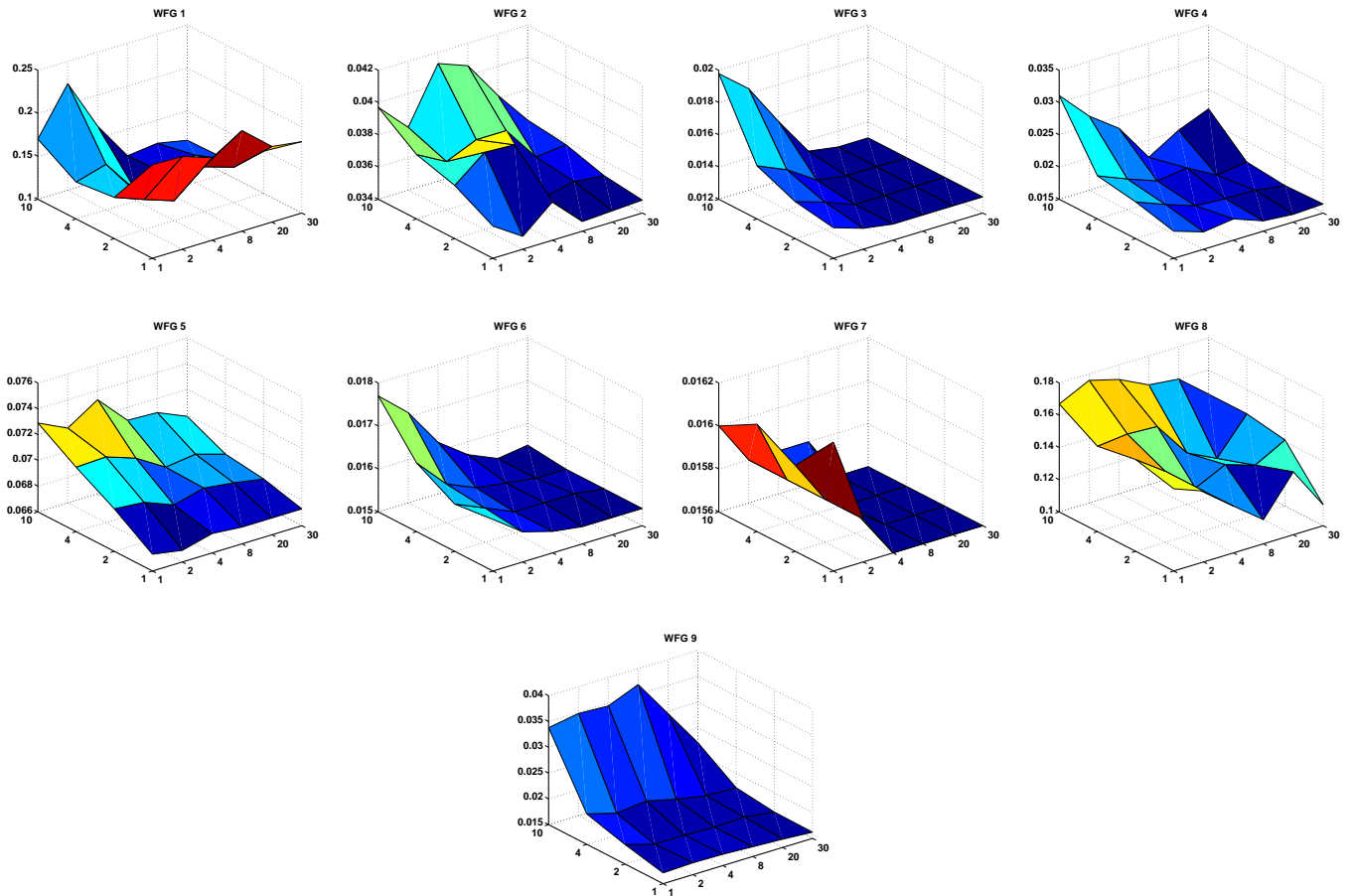


Fig. 12: Parameter sensitivity studies of K_d and ϑ .